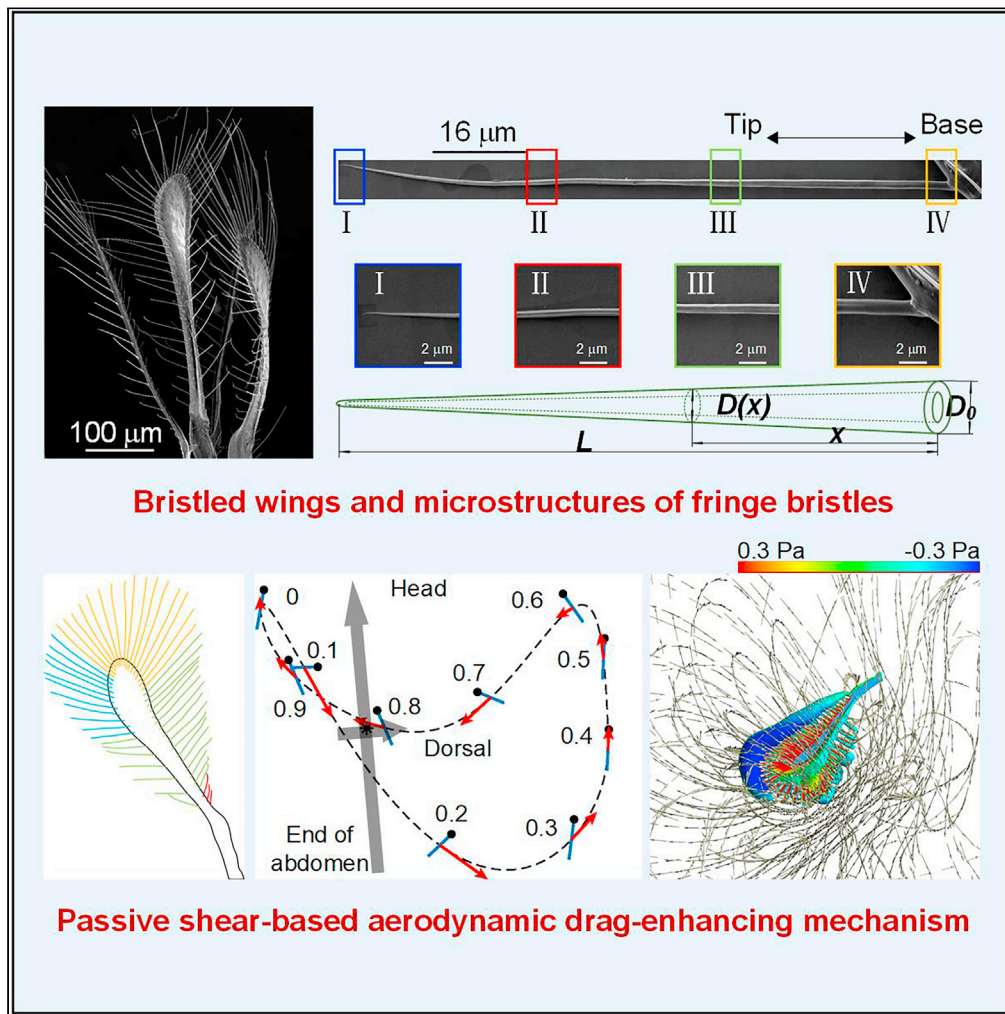


Article

Bristled-wing design of materials, microstructures, and aerodynamics enables flapping flight in tiny wasps



Yonggang Jiang,
Peng Zhao, Xuefei
Cai, ..., Xiangxiang
Jin, Deyuan
Zhang, Hao Liu

jiangyg@buaa.edu.cn (Y.J.)
pzw@suda.edu.cn (P.W.)
hliu@faculty.chiba-u.jp (H.L.)

Highlights

Bristles are extremely stiff and exhibit a high-aspect-ratio conical tubular structure

Bristles uniformize structural stress distributions and are robust to loading fatigue

Bristled wings are light, using less power to achieve novel aerodynamic force production

Bristled wings may bring an innovative design for bioinspired engineering microdevices

Jiang et al., iScience 25,
103692
January 21, 2022 © 2021 The
Authors.
[https://doi.org/10.1016/
j.isci.2021.103692](https://doi.org/10.1016/j.isci.2021.103692)



Article

Bristled-wing design of materials, microstructures, and aerodynamics enables flapping flight in tiny wasps

Yonggang Jiang,^{1,*} Peng Zhao,¹ Xuefei Cai,² Jiaxin Rong,² Zihao Dong,¹ Huawei Chen,¹ Peng Wu,^{3,*} Hongying Hu,⁴ Xiangxiang Jin,⁵ Deyuan Zhang,¹ and Hao Liu^{2,6,*}

SUMMARY

Parasitoid wasps of the smallest flying insects with bristled wings exhibit sophisticated flight behaviors while challenging biomechanical limitations in miniaturization and low-speed flow regimes. Here, we investigate the morphology, material composition, and mechanical properties of the bristles of the parasitoid wasps *Anagrus Haliday*. The bristles are extremely stiff and exhibit a high-aspect-ratio conical tubular structure with a large Young's modulus. This leads to a marginal deflection and uniform structural stress distribution in the bristles while they experience high-frequency flapping-induced aerodynamic loading, indicating that the bristles are robust to fatigue. The flapping aerodynamics of the bristled wings reveal that the wing surfaces act as porous flat paddles to reduce the overall inertial load while utilizing a passive shear-based aerodynamic drag-enhancing mechanism to generate the requisite aerodynamic forces. The bristled wing may have evolved as a novel design that achieves multiple functions and provides innovative ideas for developing bioinspired engineering microdevices.

INTRODUCTION

Parasitoid wasps, one of the smallest discovered insects with a body length of less than 1 mm, exhibit remarkably sophisticated flight behaviors while challenging biomechanical limitations in miniaturization and low-speed flow regimes (Polilov, 2016; Farisenkov et al., 2020; Sane, 2016). Wasps commonly possess bristled wings with a simple, multifunctional structural design (Seale et al., 2018). The bristled wings consist of a wing pad or rod and numerous high-aspect-ratio bristles (length (40–200 μm) to diameter (2 μm) ratio of 20 or larger) on the fringes (Figure 1A) (Polilov, 2016; Farisenkov et al., 2020). The bristles on miniature insect wings have been hypothesized to facilitate the folding and unfolding of the wings (Ellington, 1980), reduce wing inertia (Sunada et al., 2002; Kolomenskiy et al., 2020), enhance aerodynamic performance (Cummins et al., 2018; Jones et al., 2016; Santhanakrishnan et al., 2014; Davidi and Weihs, 2012), and act as mechanosensory structures (Valmalette et al., 2015). However, it is unclear how such bristled-wing morphologies and biomechanical limitations of miniature insects and their flight capabilities in particular cope with such extreme reductions in size from an integrated standpoint of materials, microstructures, and aerodynamics at low Reynolds numbers (Re , ratio of inertia to viscous force).

Biomechanical challenges in miniature insects mainly pertain to the manner, in which these insects cope with extremely high viscous losses in low- Re regimes. For instance, wasps are normally known to fly at $Re < 40$ based on the mean chord length of their bristled wings (Dudley, 2000), and they are able to overcome large viscous forces to stay airborne because of the lack of inertia. They continuously flap their wings at nearly maximum wing amplitudes to realize the advantages of the clap-and-fling mechanism (Jones et al., 2016; Santhanakrishnan et al., 2014; Weis-Fogh, 1973), which constrains the adjustment of the wingbeat frequency and has high energetic costs. It can be hypothesized that the high energetic costs may be mitigated through the morphological adaptations of the bristled and porous wings, which may generate the requisite aerodynamic forces while considerably reducing the inertial load. A main feature of three-dimensional bristled wings is their porosity (Ford et al., 2019; Strong et al., 2019), which may allow the wing surfaces to act as continuous solid plates or porous layers, thereby providing aerodynamic benefits (Jones et al., 2016). A passive flight mechanism based on a bundle of drag-enhancing bristles was recently discovered in dandelions (Cummins et al., 2018), pointing to the aerodynamic

¹Institute of Bionic and Micro-nano Systems, School of Mechanical Engineering and Automation, Beihang University, Beijing, 100191, China

²Graduate School of Engineering, Chiba University, Chiba, 263-8522, Japan

³School of Mechanical and Electrical Engineering, Soochow University, Suzhou 215021, China

⁴College of Life Science and Technology, Xinjiang University, Urumqi 830046, China

⁵Guangdong Key Laboratory of Animal Conservation and Resource Utilization, Institute of Zoology, Guangdong Academy of Sciences, Guangzhou 510260, China

⁶Lead contact

*Correspondence: jiangyg@buaa.edu.cn (Y.J.), pwu@suda.edu.cn (P.W.), hliu@faculty.chiba-u.jp (H.L.)
<https://doi.org/10.1016/j.isci.2021.103692>



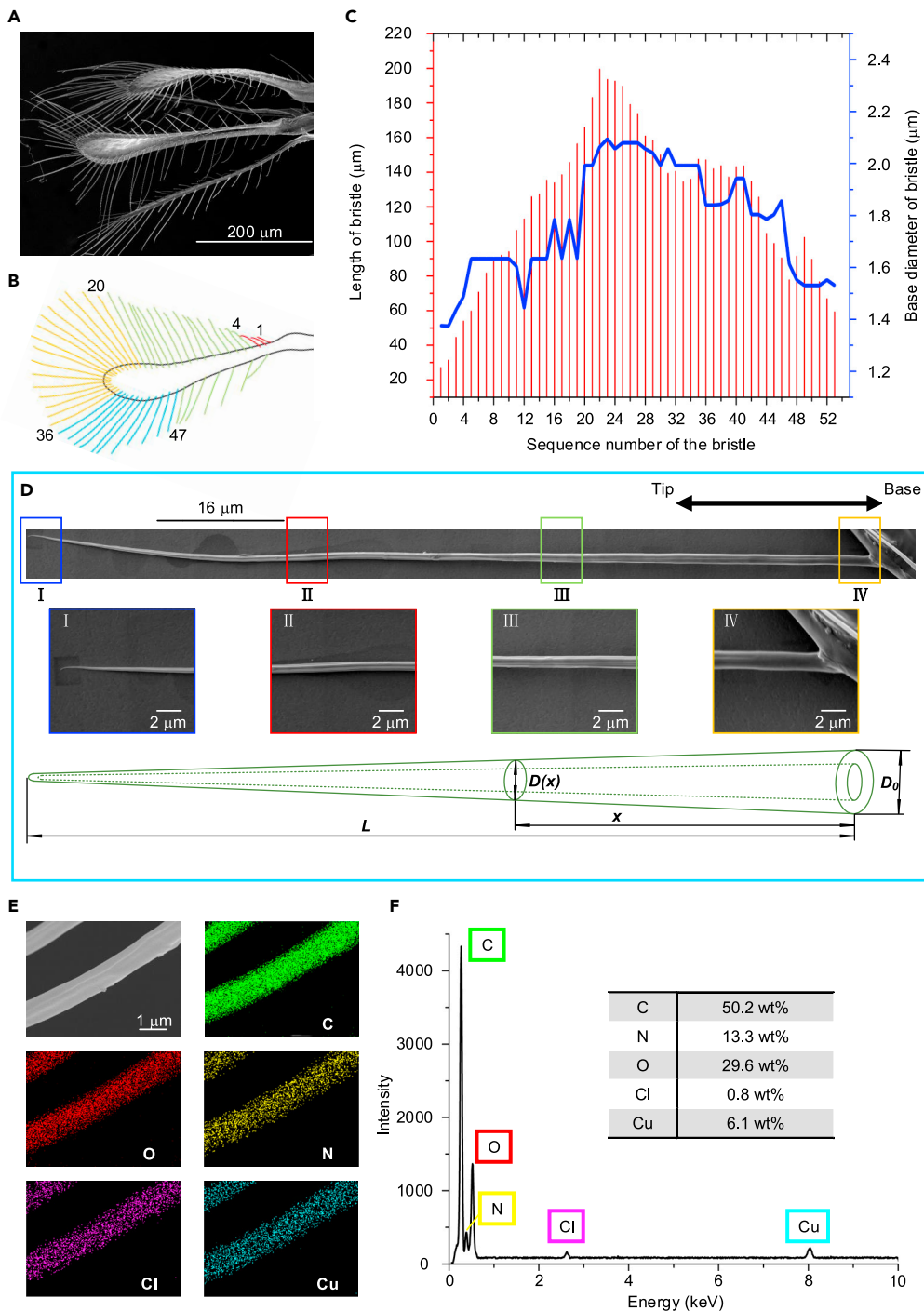


Figure 1. Morphological characteristics and materials of bristled wings and fringe bristles

(A) SEM image of pair of fore and hind wings.

(B) Schematic bristled wing with different base diameters indicated in different colors (red for $D_0 \approx 1.4 \mu\text{m}$, green for $D_0 \approx 1.6 \mu\text{m}$, blue for $D_0 \approx 1.8 \mu\text{m}$, and orange for $D_0 \approx 2.0 \mu\text{m}$).

(C) Lengths and base diameters of fringe bristles vs. sequence numbers shown in (B).

(D) SEM image of individual bristle and its geometric model, showing high-aspect-ratio conical tubular structure.

(E) EDS maps of elements C, N, O, Cl, and Cu on bristle surface.

(F) EDS spectrum of fringe bristle and elemental concentrations (inset), showing copper-enriched chitin-based biomaterial.

benefits of a stable bristle-induced separated vortex ring; however, this mechanism was observed at a considerably higher Re , specifically, $Re > 200$. Flying at low- Re conditions may be beneficial to the bristled wings of tiny insects in terms of some distinct drag-based mechanisms (Jones et al., 2016; Miller and Peskin, 2009; Ford et al., 2019; Kolomenskiy et al., 2020). However, all previous experimental and computational studies were based on highly simplified wing morphology with idealized wing motion. It thus remains poorly understood how the porous wings, distinguished from membranous wings as observed in most large insects, enable the aerodynamic force production of approximately 70%–90% of the wing load of a solid plate with a mere 10%–30% of the wing area or materials (Ellington, 1980; Sunada et al., 2002; Santhanakrishnan et al., 2014; Liu et al., 2016).

Another challenge is to uncover the material and micromechanical structural design of bristles (Seale et al., 2018). The long hair-like structure of bristles has been hypothesized to be flexible, whereas the flexural rigidity of high-aspect-ratio bristles exhibits a sensitive dependence on variations in microstructures and material properties (e.g., Young's modulus). The bristles are conventionally considered to have a Young's modulus in the range of 8–10 GPa and are morphologically characterized as cylindrical structures in most previous studies on their structural mechanics and aerodynamics (Seale et al., 2018; Jones et al., 2016). However, it has been recently observed that the fringe bristles exhibit little bending deflections (Yavorskaya et al., 2019; Zhao et al., 2019) while large variation in the wing orientation in wing beat stroke (Polilov, 2016; Cheng and Sun, 2018). The micromechanical limitations of fringe bristles are poorly understood; for instance, it is unclear whether the bristles of wasps are sufficiently stiff to suppress bristle deflections and hence variations in the wing area during flapping flight, and how the tapered tubular structures in bristles control the microstructural strength and fatigue levels.

In this study, the extreme biomechanical design of the bristled wings of the parasitoid wasps *Anagrus Haliday* (Hymenoptera: Mymaridae) was explored from a multifunctional standpoint. We first measured the material composition and morphological characteristics of the bristles and examined the Young's modulus of a single bristle. Next, using realistic mechanical properties of the bristles and realistic morphological characteristics of the bristled wing, we performed three-dimensional fluid–structure interaction (FSI) and computational fluid dynamics (CFD) modeling of flapping flights to analyze the micromechanical characteristics and sophisticated aerodynamics of the wasps. This study is the first to develop an integrated understanding of the material properties, microstructural mechanics, and low- Re aerodynamics associated with wasp flights, thus unveiling the biomechanical design principles associated with the bristled wings of wasps that help the wasps to cope with the extreme reductions in size.

RESULTS

Morphological characteristics and materials of bristles

We collected specimens of *Anagrus Haliday* (Hymenoptera: Mymaridae) and examined the morphological characteristics of their bristles, as illustrated in scanning electron microscopy (SEM) images (Figures 1A and S1) and a schematic model of the bristled wing (Figure 1B). Based on the lengths and base diameters (Figure 1C) measured in four regions (Figure 1D), the aspect ratios of the bristles were estimated and found to be extremely high: 21–35 for the red region ($D_0 \approx 1.4 \mu\text{m}$), 33–85 for the green region ($D_0 \approx 1.6 \mu\text{m}$), 67–92 for the blue region ($D_0 \approx 1.8 \mu\text{m}$), and 49–80 for the orange region ($D_0 \approx 2.0 \mu\text{m}$). The bristles were observed to have a conical tubular structure (Figure 1D) tapering toward the tip, with an inner-to-outer diameter ratio α of approximately 0.6 (Figure S1C). The structure could be fitted empirically in terms of the base diameter D_0 , length L , and shape index m , such that the outer diameter $D(x)$ at a certain position that was distance x away from the base could be defined as (Kumagai et al., 1998)

$$D(x) = D_0 \left(1 - \frac{x}{L}\right)^{\frac{1}{m}} \quad (\text{Equation 1})$$

The geometrical model showed a fine fit with the actual structure of the bristles with a shape index $m = 2.56$ (Figure S2). Using energy dispersive spectroscopy (EDS), we further examined the material composition of the bristles and confirmed that five primary elements—C, N, O, Cl, and Cu—were evenly distributed on the bristle surface (Figure 1E). These elements had distinct mass percentages in the bristles, showing copper-enriched chitin-based biomaterial (Figure 1F). These morphological and material composition characteristics of the bristles demonstrate the novel biomaterial and biomorphological design in miniature insects, and these characteristics can dominate their mechanical properties and structural strength.

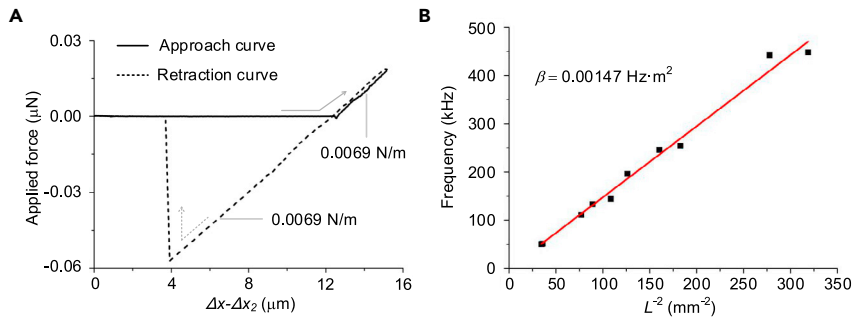


Figure 2. Mechanical properties of individual bristles

(A) Force–displacement relationship of single bristle based on AFM measurements, displaying hysteresis feature shown by arrows.

(B) Natural frequency (f) of 10 fringe bristles measured by LDV as function of bristle length (L), showing linear fit between f and L^{-2} .

Micromechanical properties of the bristles

To tackle the challenges of measuring the mechanical properties of a single bristle, we employed an experimental setup based on atomic force microscopy (AFM) for performing a bending test (Figure S3A). We explored the force–displacement correlation for an individual bristle (orange region in Figure 1B); for this purpose, a piezoelectric scanner was combined with a position-sensitive detector (PSD) (Note S1) to determine the bristle deflection (Figure 2A) under an applied force, in which the displacement of the cantilever Δx was determined by the PZT scanner, and the deflection of the cantilever Δx_2 was acquired by the PSD. For an individual bristle (e.g., length: 144 μm , base diameter: 2.0 μm), the force–displacement curve exhibited a hysteresis feature, which provided an apparent spring constant of the bristle, k_b (i.e., the tangent to the curve) as approximately 0.0069 N/m; hence, the Young’s modulus E of the bristle was derived as

$$E = k_b \int_0^L \frac{64(L-x)^2}{\pi D_0^4 \left(1 - \frac{x}{L}\right)^{4/m} (1 - \alpha^4)} dx \quad (\text{Equation 2})$$

and E was found to be 21.0 GPa. The calculated values of Young’s modulus E for all the three specimens were in the range of 18.6–23.2 GPa (Note S1, Figure S4).

To ensure the accurate estimation of Young’s modulus, we further performed contact-free deflection measurements of the bristles (Sterbing-D’Angelo et al., 2016). By using a laser Doppler vibrometer (LDV) (Figure S3B), we measured the natural frequencies of 10 bristles with a base diameter of 2.0 μm and a length range of 56–170 μm (Figures S5A–S5J). As shown in Figure 2B, the measured natural frequencies f could be well fitted, as a function of L^{-2} ($f = \beta L^{-2}$), in a linear manner with a slope of $\beta = 0.00147$ (Hz m^2). Young’s modulus was then estimated as (Note S2, Figures S6)

$$E = \frac{5.177 \pi^2 \rho D_0^{-2}}{1 + \alpha^2} \beta^2 \quad (\text{Equation 3})$$

For the density $\rho = 1.1$ kg/m^3 and $\alpha = 0.6$, Young’s modulus was calculated to be 22.3 GPa, which was in excellent agreement with that obtained from the mechanical bending test. Interestingly, for the highest aspect ratio in the range of 67–92 (Figures 1B, S7, and S8), the bristles in wasps exhibited an astonishingly stiff mechanical property, which doubled Young’s modulus in the range of 8–10 GPa, as reported in previous studies (Seale et al., 2018). Thus, it is reasonable to suggest that the bristled wing may have micromechanical and aerodynamic benefits owing to the high stiffness, high aspect ratio, and conical tubular structure of the hair-like bristles.

Micromechanical and aerodynamic benefits of bristles

Through the fluid–bristle interaction modeling (Figure 3A) of a wasp-inspired bristled wing experiencing aerodynamic loading induced by high-frequency flapping, we tackled a central question on the extreme micromechanical design of the bristled wings: how the tapered tubular structure in bristles controls the

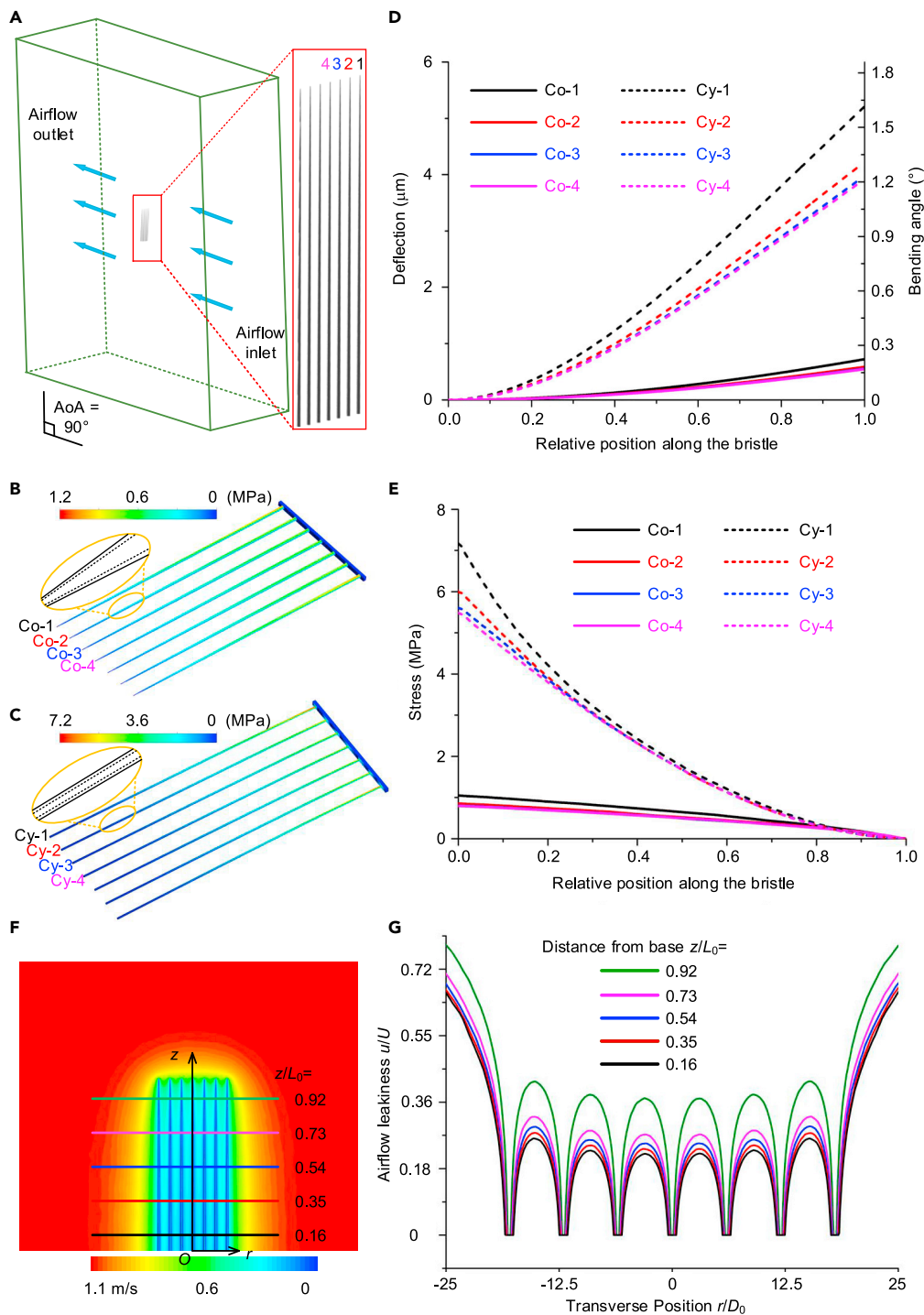


Figure 3. Micromechanical and aerodynamic characteristics of bristled-wing model

- (A) Schematic of fluid–bristle interaction model with seven bristles translating in inflow of 1.1 m/s at AoA of 90°C.
 (B) Stress distributions in realistic conical tubular wing model.
 (C) Stress distributions in cylindrical tubular wing model.
 (D) Deflections vs. length in bristles.
 (E) Stress distributions vs. length in bristles.
 (F) In-plane iso-airflow speed contours of bristled wing.
 (G) Airflow velocity distributions at five cross sections (corresponding to five colored lines in (F)).

microstructural strength and fatigue levels. In contrast to conventional solid cylindrical bristle models (Jones et al., 2016; Weihs and Barta, 2008), a novel three-dimensional bristled wing model (Figure 3B) was developed, which comprised seven individual bristles in the form of a bristle array based on the measured morphological characteristics of the conical tubular structure and the mechanical properties of the realistic bristles (as summarized in Table S1); each individual bristle was set apart with an interval equaling six times the bristle base diameter ($G/D = 6$, G refers to the gap between bristles and D their base diameter, respectively) (Jones et al., 2016). A cylindrical tubular model (Figure 3C) with an outer diameter of $1.17 \mu\text{m}$ was also constructed for comparison, so that the bristle volume was conserved with that of the conical tubular model. For an inflow of 1.1 m/s (Note S3) at an angle of attack (AoA) of 90° with the maximum flapping-wing aerodynamic loading (Figure 3A), the realistic bristles were observed to deflect marginally, exhibiting a maximum deflection of $0.7 \mu\text{m}$ and a bending angle of 0.22° for Bristle Co-1 (Figure 3D). For the cylindrical model, the deflection and bending angle increased up to seven times of $5.2 \mu\text{m}$ and 1.61° . It is thus reasonable to infer that the stiff bristled wing likely benefits from the marginal deflection to sustain the maximum wing area during flapping flight, which is supported by the recent observations that the fringe bristles of tiny insects in flapping flight exhibit little bending deflections (Yavorskaya et al., 2019; Zhao et al., 2019) while large variation in the wing orientation (Polilov, 2016; Cheng and Sun, 2018). Moreover, the conical tubular bristles exhibited a considerably lower and uniform stress distribution (Figures 3B–3E) longitudinally with the maximum stress, which was one order lower than that of the cylindrical model (Figures 3C–3E). This indicates the sophisticated micromechanical benefits of the enhanced structural strength and long-life fatigue in bristles.

The aerodynamic benefits of the bristled wings were explored by examining how the porosity of the bristled wings could resolve a tradeoff between airflow leakiness and wing area reduction. By using a mere 10%–30% of the area of a solid-plate (membrane) wing or by causing a 70%–90% reduction in the wing area and used materials (Ellington, 1980; Sunada et al., 2002; Jones et al., 2016; Santhanakrishnan et al., 2014; Kolomenskiy et al., 2020), we found that the bristled wing could apparently facilitate the formation of a thick, low-speed boundary layer (Figure 3F) ($\delta \propto \sqrt{1/Re}$, where δ is the thickness of the boundary layer). The boundary layer wrapped up the entire wing surface while exhibiting an averaged airflow leakiness (u/U , where u denotes the calculated velocity between the bristles, and U the inlet velocity of 1.1 m/s , respectively) of 0.26–0.42 in variation with the G/D ranging from 6 to 16 along the axis z (Figure 3G). This is consistent with those in the previous study (Jones et al., 2016), where the averaged airflow leakiness was reported to be ~ 0.2 and ~ 0.4 with G/D of 5 and 15, respectively. These features are consistent with those of previous simulations (Cheng and Sun, 2018; Barta and Weihs, 2006; Aram et al., 2013; Kolomenskiy et al., 2020). This implies that the porous wing may effectively minimize the airflow leakiness owing to the low- Re flow (Santhanakrishnan et al., 2014; Weis-Fogh, 1973; Kolomenskiy et al., 2020), enabling sufficient aerodynamic force production while reducing the inertial load.

Low- Re flapping aerodynamics of realistic bristled wings

Here, we examined the bristle-induced unsteady aerodynamic mechanisms in association with a single bristled wing through the CFD modeling of three sophisticated models with realistic configurations of the wing and bristles: a bristled wing (BW), a membranous (flat plate) wing (MW), and a small wing (SW), which underwent realistic flapping-wing motions observed in a tiny wasp (Figure 4A). The realistic BW (Figure 4B) had the same number and length of the fringe bristles, as shown in Figures 1C and 1D; the MW was a flat plate enveloping the outline of the BW (Figure 4C); and the SW has a wing area integrating the central rod and an additional portion equivalent to a projected area of all the fringe bristles in the BW (Figure 4D). It is worth noting that a single bristled wing model is employed here rather than a paired wing because we aim to unveil the essential underlying aerodynamic mechanism associated with the mere bristled wing without consideration of the clap-and-fling effects.

Based on the flapping-wing kinematics in wasps (Ellington, 1980; Jones et al., 2016; Cheng and Sun, 2018), both unsteady and steady CFD simulations were performed, with the single rigid wing models experiencing either a flapping motion during the hovering flight (identical to a Re of 16 based on the mean wing chord-length and average wingtip velocity) of a wasp (Figure 4A) or a uniform inflow of 0.5 – 2.0 m/s at an AoA of 90° at a wing chord-length-based Re of 7–30 (Figure S9). The bristle-induced airflows in the BW (Figures 4B–4E, Video S1) exhibited distinct features in the local velocities and flow topologies from the MW (Figures 4C–4F, Video S2) and SW (Figures 4D–4G, Video S3); for example, at the middle and tip cross sections during a downstroke ($t = 0.14T$), the wing porosity was reconfirmed to be capable of

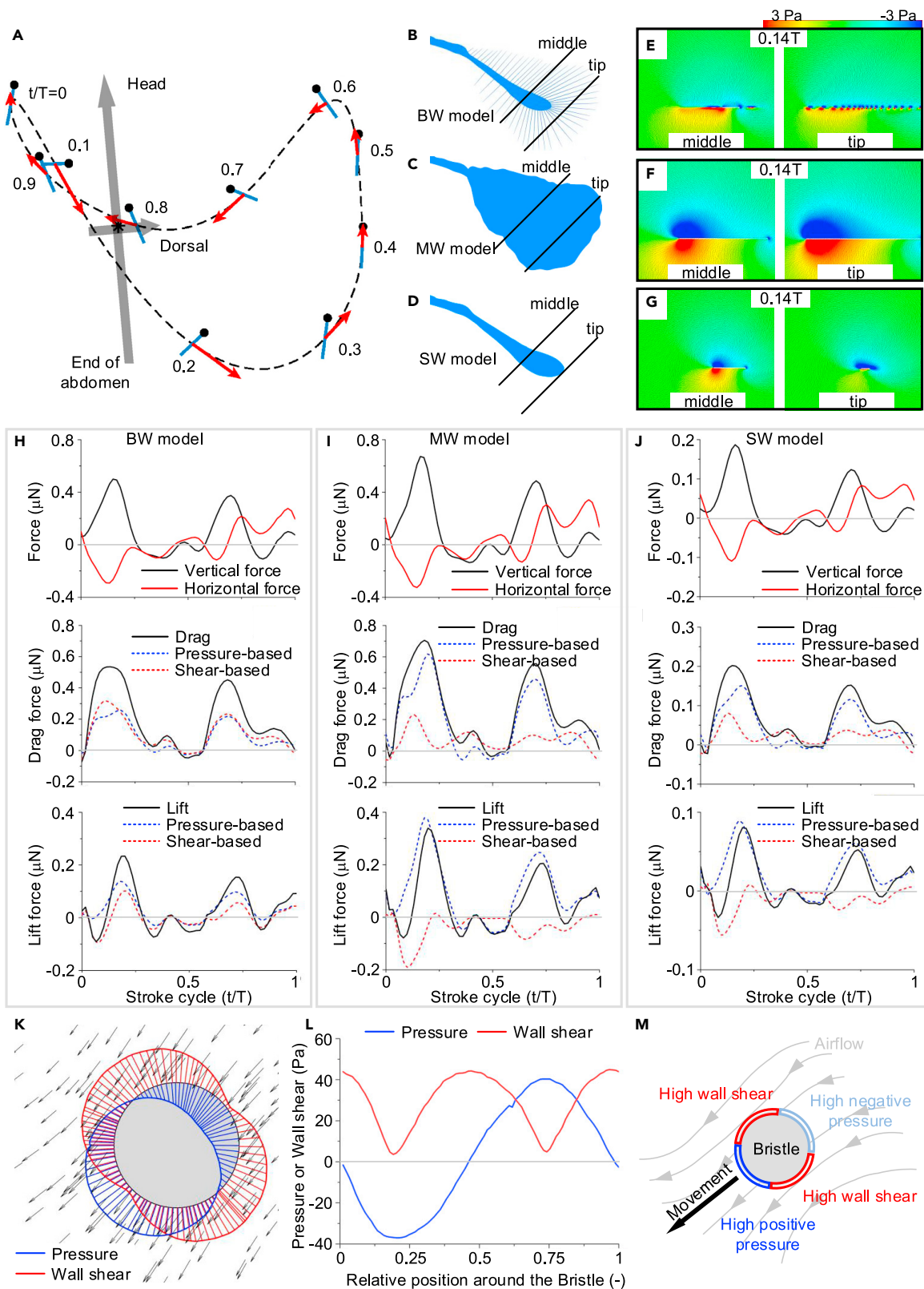


Figure 4. Flapping aerodynamics of three CFD models with realistic configurations of wing and bristles

- (A) Flapping-wing motion of tiny wasp reproduced from (Cheng and Sun, 2018).
- (B) BW, with realistic configurations of wing and bristles.
- (C) MW, flat-plate wing enveloping outline of BW.
- (D) SW, with projected wing area equal to that of BW. The three wing models experience the same flapping motion (A).
- (E–G) Pressure distributions and velocity vectors of BW, MW, and SW, respectively, at middle and tip cross sections in spanwise direction ($t = 0.14T$).
- (H–J) Time courses of vertical, horizontal, drag, and lift forces as well as pressure- and shear-based drag and lift force components in one stroke cycle for BW, MW, and SW models, respectively.
- (K) Velocity vectors about single bristle and distributions of wall shear stress and pressure on surface ($t = 0.14T$).
- (L) Transient wall shear stresses and pressures on the surface in one stroke cycle.
- (M) Schematic diagram of pressure-based and wall shear-stress-based drags on bristle surface.

passively manipulating the airflow leakiness penetrating the porous wings to a considerably suppressed portion. This behavior is consistent with that in the wasp-inspired wing model (Figure 3) as well as in a rotary wing model (Kolomenskiy et al., 2020) and further leads to a globally similar but locally differential pressure map/distribution, unlike the distribution for the fan-like MW (Figures 4C–4F, Videos S1–S3). The fringe bristles distributed as an array *in toto* facilitated the formation of an overall pressure field around the bristled wing, which was apparently induced by a membrane sharing the same outline and area of the fringe portion. The time courses of the three wing models showed a similar trend in aerodynamic force production, including vertical and horizontal forces (Figures 4H–4J). However, the BW could create a cycle-mean vertical force of 0.1026 mN per wing in a wing stroke (Table S3), which was approximately 82% of that (0.1249 mN per wing) of the MW (Table S3). This force was sufficiently large to support the average weight (0.194 mN) of wasps (Farisenkov et al., 2020; Weis-Fogh, 1973; Cheng and Sun, 2018), while providing a 76% reduction in the wing area (Table S2). When the fringe bristles were removed from the central rod of the wing in the SW (Figure 4C), the flow structures changed substantially (Figure 4G), resulting in a 76% decline in the cycle-mean vertical force (0.0298 mN per wing) (Figure 4J and Table S3).

Unlike the high- Re ($100 < Re < 10,000$) aerodynamics (Liu et al., 2016) in flapping flights, the low- Re (< 40) aerodynamics apparently benefited from an underlying drag-based mechanism in addition to the lift-based mechanism (Jones et al., 2016; Kolomenskiy et al., 2020), as illustrated in Figures 4H–4J; the drag forces of the BW, MW, and SW models were considerably greater than the lift forces over a wing stroke, achieving cycle-mean drag-to-lift ratios of 6.1, 4.4, and 5.9, respectively. The drag and lift forces were composed of pressure-based (normal to the wall surface) and shear-stress (or friction)-based (tangent to the wall surface) force components. Our results (Figures 4H–4J) demonstrated that in a wing stroke, the bristle-induced drag forces of the BW contained almost equal contributions from pressure (0.0918 mN) and shear stress (0.1113 mN), whereas the drag forces in the membranous wings of the MW and SW were primarily pressure-based (0.1849 mN in the MW), with considerably less contribution from the shear stress (0.0673 mN in the MW), which even had a negative effect on the lift force production (Figure 4I and Table S3). Thus, our results confirmed that the fringe bristles demonstrate the drag-based mechanism in terms of passively enhancing the viscous shear-stress-based force production to mitigate the loss in the pressure-based forces (Santhanakrishnan et al., 2014; Ford et al., 2019; Strong et al., 2019). Shear stress or friction-based drags at high Re are proportional to the wet surface upon which they act. It has been reported (Santhanakrishnan et al., 2014; Kolomenskiy et al., 2020) that the flow passing through the bristles is responsible for enhancing the shear stress-induced drag production. This was further examined here by investigating the pressure-based or shear-stress-based contributions to the drag force acting on a single bristle. It is verified that given the remarkable 76% reduction in the wing area, the BW apparently outperformed the MW in terms of the shear-stress-based drag production, with a 65% increase in the cycle-mean shear-stress-based drag (Table S3). For example, we considered a bristle at the wing tip of the BW (Figure 4B). The pressure and shear stress distributions around a circular cylinder demonstrated the existence of a pair of high wall shear zones (marked in red) responsible for augmenting the friction-based drag production; the pressure difference between the front and rear parts (marked in blue) contributed to the pressure-based drag (Figures 4K–4M). This further explained why the pressure-based and viscous shear-stress-based components contributed equally to the bristle-induced drag forces, as shown in Figure 4H and Table S3, indicating an alternative low- Re aerodynamic mechanism that was different from the lift-based high- Re aerodynamic mechanisms (Liu et al., 2016) and the drag-enhancing pappus of dandelion seeds (Cummins et al., 2018). Moreover, this mechanism was highly efficient and capable of achieving a remarkable reduction in the viscous loss and hence the energetic cost (Figure S10). As listed in Tables S2 and S3, a 76% reduction in the BW's wing area led to an 81% drop in the inertial power compared with that of the MW, and hence, a 70% reduction was achieved in the

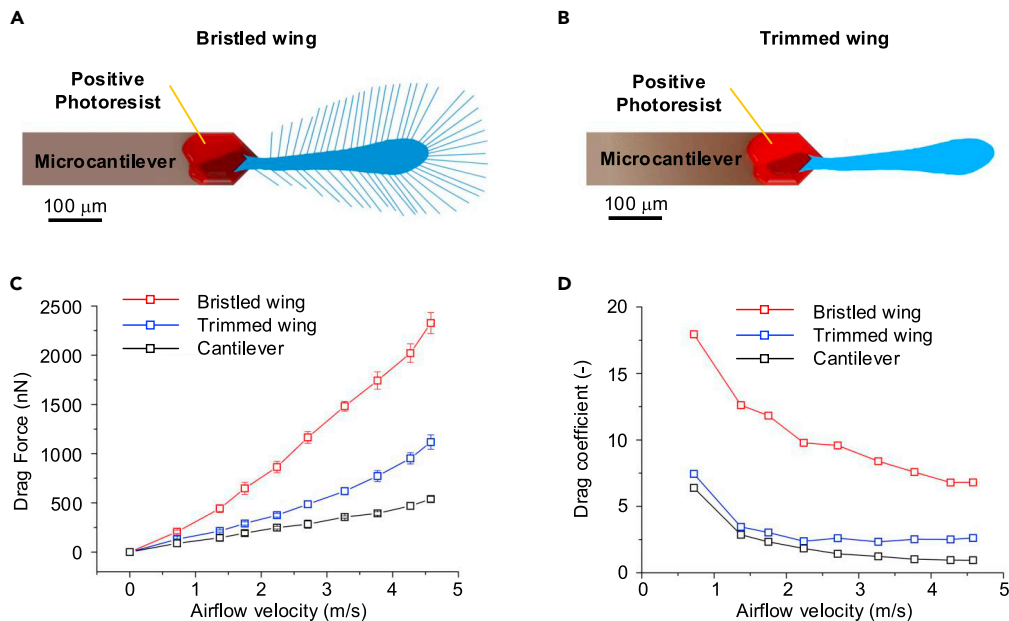


Figure 5. Measured drag forces acting on bristled wing with piezo resistive cantilever
(A) Schematic of cantilever mounted onto bristled wing.
(B) Bristled wing after laser trimming.
(C) Drag forces vs. inflow velocities. Error bars show standard deviation of three experimental runs.
(D) Drag coefficients vs. inflow velocities.

total power, including inertial and aerodynamic powers. While the membranous wings needed to pay a considerable cost in terms of the inertial power rather than the aerodynamic power, e.g., 4.3 times in the MW and 3.4 times even in the SW, thus, the BW could achieve a low cost in terms of both the inertial and aerodynamic power consumptions (Table S3).

The effectiveness of the bristled wing in producing high aerodynamic drag force with lower wing area was further confirmed by wind tunnel tests (Figure S11). The measured aerodynamic forces acting on a real bristled wing at an AoA of 90° show the same trend in terms of drag force vs airflow velocity as obtained in the steady simulations (Figure S9). In a low-speed wind tunnel, we employed a self-sensing piezoresistive microcantilever to measure drag forces on a real wing with fringe bristles (Figure 5A) and a wing with the bristles removed by laser trimming (Figure 5B) in a velocity range of 0–4.58 m/s (Note S5). We found that the bristled wing produced a drag force that was 2.9–4.9 times greater than that produced by the trimmed wing (Figure 5C). This increase corresponded to a remarkable rise in the drag coefficients by 2.4–4.1 times (Figure 5D). Overall, these results were consistent with the CFD-based results and conclusions (Figure S9).

DISCUSSION

The primary biomechanical challenge in miniature insects is to cope with the extremely high viscous loss in low-*Re* regimes. In this regard, we discovered that the bristled and porous wings in wasps benefit from a sophisticated aerodynamic design to achieve a passive bristle-induced, shear-based drag-enhancing mechanism, leading to a remarkable reduction in energetic cost, while resolving a tradeoff between airflow leakiness and wing-inertia reduction. The drag-based mechanism associated with the wings with fringe bristles in small insects is considered as a primary aerodynamic principle in the low-*Re* flow regime (Sunada et al., 2002; Jones et al., 2016; Santhanakrishnan et al., 2014; Davidi and Weihs, 2012; Cheng and Sun, 2018; Barta and Weihs, 2006; Kolomenskiy et al., 2020) because the aerodynamic performance in terms of lift force production and lift-to-drag ratio declines dramatically owing to the large viscous losses. The mechanism has been hypothesized to be pressure-based, with the bristled wing acting as a membranous wing (e.g., a flat paddle), which results in high energetic costs because of a large wing inertial loading (Davidi and Weihs, 2012; Cheng and Sun, 2018; Weihs and Barta, 2008; Barta and Weihs, 2006; Kolomenskiy et al., 2020). Thus, there exists a tradeoff between the airflow leakiness

penetrating the bristled and porous wing surface and the wing-area-based and material-based inertia reduction. While previous studies have pointed out that the friction drag-based mechanism is responsible for answering how the bristled wings resolve the tradeoff (Ellington, 1980; Sunada et al., 2002; Cummins et al., 2018; Jones et al., 2016; Santhanakrishnan et al., 2014; Davidi and Weihs, 2012; Miller and Peskin, 2009; Cheng and Sun, 2018; Weihs and Barta, 2008; Barta and Weihs, 2006; Aram et al., 2013; Kolomenskiy et al., 2020), it still remains unclear how the novel flapping aerodynamics and energetics of the bristled wings are achieved in real wasp flight.

Although the low-Re aerodynamics pertaining to bristled wings have been studied by means of mechanically enlarged biomimetic wing models (Sunada et al., 2002; Takahashi et al., 2015; Kolomenskiy et al., 2020), theoretical analyses (Ellington, 1980; Weis-Fogh, 1973; Kawachi and Yasuda, 2003), and CFD simulations (Jones et al., 2016; Santhanakrishnan et al., 2014; Davidi and Weihs, 2012; Miller and Peskin, 2009; Cheng and Sun, 2018; Weihs and Barta, 2008; Barta and Weihs, 2006; Aram et al., 2013; Liu, 2009; Liu and Aono, 2009; Kolomenskiy et al., 2020), the morphological characteristics and material properties of fringe bristles have seldom been studied so far. This study is the first to carry out 3D CFD modeling of a realistic bristled wing mimicking wing kinematics in flapping flight and a comprehensive comparison with membranous wings. We found that the bristled wings in wasps utilize a novel drag-enhancing principle owing to a bristle-induced, shear-based mechanism while overcoming the disadvantage of losing the pressure-based drag force. This is effectively achieved through the bristled and porous wing design to reduce the overall wing inertial loading while facilitating the production of the requisite aerodynamic forces, thereby providing a novel resolution to the tradeoff. A passive drag-enhancing mechanism was recently discovered in the common dandelion in which the porosity of a bundle of bristles, i.e., the pappus, is found to stabilize a separated vortex ring while maximizing loading and minimizing material requirements under high-Re (>200) conditions (Cummins et al., 2018). However, the bristled wings in wasps are downsized to an order of 1 mm and move under low-Re (<40) conditions; the wings behave like a two-dimensional flat plate with the fringe bristles optimized in length and number, which is responsible for creating the flapping-wing aerodynamic forces that allow the insect to stay aloft. This is a new class of fluid behavior associated with fluid-bristle wings undergoing active flapping motion in the low-Re regime (Ford et al., 2019; Kolomenskiy et al., 2020; Strong et al., 2019).

The discovery of the unique material and micromechanical characteristics of the bristles further provides concrete evidence on the effectiveness and robustness of the bristle-induced, shear-based drag-enhancing mechanism. The mechanism can be enhanced effectively by increasing the wing area while maintaining a reasonable 2D configuration arrangement of the bristles during active flapping (Figures 1A and 1B), leading to the maximization of both the pressure- and shear-based drag forces. While exhibiting a conical tubular structure with a considerably high aspect ratio (Figures 1C and 1D), the fringe bristles of *Anagrus Haliday* were found to be extremely stiff with a large Young's modulus of ~ 22 GPa (Figure 2), which is more than twice the value for cuticle hairs (8–10 GPa) (Seale et al., 2018; Dirks and Dürr, 2011). The bristles were examined through fluid-bristle interaction simulations and found to have extremely high stiffness with marginal deflections, which enabled the bristled wing area to be approximately unchanged under aerodynamic loading. Such rigidity likely originates from the element concentration of the biomineral atacamite and unmineralized Cu, which shows a weight fraction of 6.1 wt% (Figure 1F) (Kramer et al., 1993; Lichtenegger et al., 2002). We measured the Young's modulus of the fringe bristles of thrips, which are also chitin-based biomaterials but without Cu, and Young's modulus was approximately 10.4 GPa (Note S6, Figure S12), which is considerably smaller than that of *Anagrus Haliday*. Note that although the insects used in the experiments were dead creatures stored in 70% ethanol, the difference in Young's modulus between fresh and dry hard insect cuticles (with low water concentrations) was confirmed to be very limited (Vincent and Wegst, 2004; Peisker et al., 2013).

The biomorphological design of the high-aspect-ratio conical tubular bristles further demonstrates the sophisticated capabilities of the insects to remarkably lower and uniformize structural stress distributions in bristles (Figures 3B–3E). Small insects such as wasps and thrips perform fast flapping at several hundred times per second, and the bristled wings normally experience both flapping-induced aerodynamic loading and clapping-induced structural mechanical loading. The unique micromechanical design that combines the stiff mechanical property and the conical tubular morphology of the bristles likely evolved as a form of optimal selection to enhance structural strength and long-life fatigue and thereby increase the robustness of flight capabilities in miniature insects.

CONCLUSION

In summary, the extreme biomechanical design of the bristled wings of wasps offers a sophisticated resolution to the tradeoff between the energetic cost and aerodynamic force production while reducing the overall inertial load. This enables miniature insects such as wasps to stay airborne by pushing the physical boundary of sizing limitations. The hair-like bristles may have evolved as a novel design that provides multiple functions of micro-mechanics and aerodynamics, and this design can provide innovative ideas for developing bioinspired engineering microdevices. The study of miniature insects thus provides exciting avenues for insect flight studies, which can possibly lead to the discovery of novel biomechanical principles. Such studies will help us understand how insects coped with and evolved from the tradeoff-based evolutionary challenges of miniaturization.

Limitations of the study

This study presents an integrated study to explore the extreme biomechanical design of the bristled wings of the parasitoid wasps through investigating the materials, microstructures, and low Reynolds number aerodynamics of the bristled wings of tiny wasps. The flapping-wing model in CFD simulations is a single bristled wing rather than a paired wing and thus the clap-and-fling effects, i.e., the wing–wing interaction is not taken into consideration.

STAR★METHODS

Detailed methods are provided in the online version of this paper and include the following:

- KEY RESOURCES TABLE
- RESOURCE AVAILABILITY
 - Lead contact
 - Materials availability
 - Data and code availability
- EXPERIMENTAL MODEL AND SUBJECT DETAILS
- METHOD DETAILS
 - SEM and EDS
 - Bending test using AFM
 - LDV measurement
 - Fluid–bristle interaction analysis
 - CFD modeling of flapping-wing flight
- QUANTIFICATION AND STATISTICAL ANALYSIS

SUPPLEMENTAL INFORMATION

Supplemental information can be found online at <https://doi.org/10.1016/j.isci.2021.103692>

ACKNOWLEDGMENTS

This work is supported by the National Natural Science Foundation of China (No. 52022008, 51975030, T2121003).

AUTHOR CONTRIBUTIONS

Y. Jiang, D. Zhang, and H. Liu conceived the project and designed the experiments. Y. Jiang and P. Zhao performed the bending tests and LDV measurements. P. Zhao, X. Cai, and Z. Dong worked on the investigation of parameters for the CFD analysis. P. Wu, X. Cai, J. Rong, and Z. Dong performed the CFD analysis. P. Zhao, H. Chen, and X. Cai collected and analyzed the data. Y. Jiang, H. Liu, and P. Zhao wrote the manuscript. H. Hu and X. Jin made the field study and collected the tiny wasps.

DECLARATION OF INTERESTS

The authors declare that they have no competing interests.

Received: September 26, 2021

Revised: November 30, 2021

Accepted: December 20, 2021

Published: January 21, 2022

REFERENCES

- Aram, S., Singh, R., and Dinavahi, S.P.G. (2013). CFD analysis of flapping wings in ultra-low Reynolds number regime. *Int. J. Micro Air Veh.* 5, 93–107. <https://doi.org/10.1260/1756-8293.5.2.93>.
- Barta, E., and Weihs, D. (2006). Creeping flow around a finite row of slender bodies in close proximity. *J. Fluid Mech.* 551, 1–17. <https://doi.org/10.1017/S0022112005008268>.
- Cheng, X., and Sun, M. (2018). Very small insects use novel wing flapping and drag principle to generate the weight-supporting vertical force. *J. Fluid Mech.* 855, 646–670. <https://doi.org/10.1017/jfm.2018.668>.
- Cummins, C., Seale, M., Macente, A., Certini, D., Mastropaolo, E., Viola, I.M., and Nakayama, N. (2018). A separated vortex ring underlies the flight of the dandelion. *Nature* 562, 414–418. <https://doi.org/10.1038/s41586-018-0604-2>.
- Davidi, G., and Weihs, D. (2012). Flow around a combwing in low-Reynolds-number flow. *AIAA J.* 50, 249–253. <https://doi.org/10.2514/1.J051383>.
- Dirks, J.H., and Dürr, V. (2011). Biomechanics of the stick insect antenna: damping properties and structural correlates of the cuticle. *J. Mech. Behav. Biomed. Mater.* 4, 2031–2042. <https://doi.org/10.1016/j.jmbbm.2011.07.002>.
- Dudley, R. (2000). *The Biomechanics of Insect Flight: Form, Function, Evolution* (Princeton University Press Publishing).
- Ellington, C.P. (1980). Wing mechanics and take-off preparation of thrips (Thysanoptera). *J. Exp. Biol.* 85, 129–136.
- Farisenkov, S.E., Lapina, N.A., Petrov, P.N., and Polilov, A.A. (2020). Extraordinary flight performance of the smallest beetles. *Proc. Natl. Acad. Sci. U S A* 117, 24643–24645. <https://doi.org/10.1073/pnas.2012404117>.
- Ford, M.P., Kasoju, V.T., Gaddam, M.G., and Santhanakrishnan, A. (2019). Aerodynamic effects of varying solid surface area of bristled wings performing clap and fling. *Bioinspiration and Biomimetics* 14, 046003. <https://doi.org/10.1088/1748-3190/ab1a00>.
- Jones, S.K., Yun, Y.J.J.J., Hedrick, T.L., et al. Yun, Y.J.J.J., Jones, S.K., Miller, L.A., Yun, Y.J.J.J., Hedrick, T.L., Griffith, B.E., Miller, L.A. (2016). Bristles reduce the force required to ‘fling’ wings apart in the smallest insects. *J. Exp. Biol.* 219, 3759–3772. <https://doi.org/10.1242/jeb.143362>.
- Kawachi, K., and Yasuda, K. (2003). Advantages of a bristled wing as a rotary wing. *J. Aircr.* 40, 1000–1002. <https://doi.org/10.2514/2.6887>.
- Kolomenskiy, D., Farisenkov, S., Engels, T., Lapina, N., Petrov, P., Lehmann, F.O., Onishi, R., Liu, H., and Polilov, A. (2020). Aerodynamic performance of a bristled wing of a very small insect: dynamically scaled model experiments and computational fluid dynamics simulations using a revolving wing model. *Exp. Fluids* 61, 1–13. <https://doi.org/10.1007/s00348-020-03027-0>.
- Kramer, R., Lehn, J.M., and Marquis-Rigault, A. (1993). Self-recognition in helicate self-assembly: spontaneous formation of helical metal complexes from mixtures of ligands and metal ions. *Proc. Natl. Acad. Sci. U S A* 90, 5394–5398. <https://doi.org/10.1073/pnas.90.12.5394>.
- Kumagai, T., Shimozawa, T., and Baba, Y. (1998). The shape of wind-receptor hairs of cricket and cockroach. *J. Comp. Physiol. - A. Sensory, Neural Behav. Physiol.* 183, 187–192.
- Lichtenegger, H.C., Schöberl, T., Bartl, M.H., Waite, H., and Stucky, G.D. (2002). High abrasion resistance with sparse mineralization: copper biomineral in worm jaws. *Science* 298, 389–392. <https://doi.org/10.1126/science.1075433>.
- Liu, H. (2009). Integrated modeling of insect flight: from morphology, kinematics to aerodynamics. *J. Comput. Phys.* 228, 439–459. <https://doi.org/10.1016/j.jcp.2008.09.020>.
- Liu, H., and Aono, H. (2009). Size effects on insect hovering aerodynamics: an integrated computational study. *Bioinspiration and Biomimetics* 4, 015002. <https://doi.org/10.1088/1748-3182/4/1/015002>.
- Liu, H., Ravi, S., Kolomenskiy, D., and Tanaka, H. (2016). Biomechanics and biomimetics in insect-inspired flight systems. *Philos. Trans. R. Soc. B Biol. Sci.* 371, 20150390. <https://doi.org/10.1098/rstb.2015.0390>.
- Miller, L.A., and Peskin, C.S. (2009). Flexible clap and fling in tiny insect flight. *J. Exp. Biol.* 212, 3076–3090. <https://doi.org/10.1242/jeb.028662>.
- Peisker, H., Michels, J., and Gorb, S.N. (2013). Evidence for a material gradient in the adhesive tarsal setae of the ladybird beetle *Coccinella septempunctata*. *Nat. Commun.* 4, 1607–1608. <https://doi.org/10.1038/ncomms2576>.
- Polilov, A.A. (2016). *At the Size Limit-Effects of Miniaturization in Insects* (Springer Publishing).
- Sane, S.P. (2016). Neurobiology and biomechanics of flight in miniature insects. *Curr. Opin. Neurobiol.* 41, 158–166. <https://doi.org/10.1016/j.conb.2016.09.008>.
- Santhanakrishnan, A., Robinson, A.K., Jones, S., Low, A.A., Gadi, S., Hedrick, T.L., and Miller, L.A. (2014). Clap and fling mechanism with interacting porous wings in tiny insect flight. *J. Exp. Biol.* 217, 3898–3909. <https://doi.org/10.1242/jeb.084897>.
- Seale, M., Cummins, C., Viola, I.M., Mastropaolo, E., and Nakayama, N. (2018). Design principles of hair-like structures as biological machines. *J. R. Soc. Interf.* 15, 20180206. <https://doi.org/10.1098/rsif.2018.0206>.
- Sterbing-D’Angelo, S.J., Liu, H., Yu, M., and Moss, C.F. (2016). Morphology and deflection properties of bat wing sensory hairs: scanning electron microscopy, laser scanning vibrometry, and mechanics model. *Bioinspiration and Biomimetics* 11, 056008. <https://doi.org/10.1088/1748-3190/11/5/056008>.
- Strong, E.F., Pezzulla, M., Gallaire, F., Reis, P., and Siconolfi, L. (2019). Hydrodynamic loading of perforated disks in creeping flows. *Phys. Rev. Fluids* 4, 1–22. <https://doi.org/10.1103/PhysRevFluids.4.084101>.
- Sunada, S., Takashima, H., Hattori, T., Yasuda, K., and Kawachi, K. (2002). Fluid-dynamic characteristics of a bristled wing. *J. Exp. Biol.* 205, 2737–2744.
- Takahashi, H., Sato, K., Nguyen, M.D., Matsumoto, K., and Shimoyama, I. (2015). Characteristic evaluation of a bristled wing using mechanical models of a thrips wings with MEM piezoresistive cantilevers. *J. Biomech. Sci. Eng.* 10, 1–10. <https://doi.org/10.1299/jbse.14-00233>.
- Valmalette, J.C., Raad, H., Qiu, N., Ohara, S., Capovilla, M., and Robichon, A. (2015). Nano-architecture of gustatory chemosensory bristles and trachea in *Drosophila* wings. *Sci. Rep.* 5, 14198. <https://doi.org/10.1038/srep14198>.
- Vincent, J.F.V.V., and Wegst, U.G.K.K. (2004). Design and mechanical properties of insect cuticle. *Arthropod Struct. Dev.* 33, 187–199. <https://doi.org/10.1016/j.asd.2004.05.006>.
- Weihs, D., and Barta, E. (2008). Comb wings for flapping flight at extremely low Reynolds numbers. *AIAA J.* 46, 285–288. <https://doi.org/10.2514/1.32500>.
- Weis-Fogh, T. (1973). Quick estimates of flight fitness in hovering animals, including novel mechanisms for lift production. *J. Exp. Biol.* 59, 169–230.
- Yavorskaya, M.I., Beutel, R.G., Farisenkov, S.E., and Polilov, A.A. (2019). The locomotor apparatus of one of the smallest beetles—the thoracic skeletomuscular system of *Nephanes titan* (Coleoptera, Ptiliidae). *Arthropod Struct. Dev.* 48, 71–82. <https://doi.org/10.1016/j.asd.2019.01.002>.
- Zhao, P., Dong, Z., Jiang, Y., Liu, H., Hu, H., Zhu, Y., and Zhang, D. (2019). Evaluation of drag force of a thrip wing by using a microcantilever. *J. Appl. Phys.* 126. <https://doi.org/10.1063/1.5126617>.

STAR★METHODS

KEY RESOURCES TABLE

REAGENT or RESOURCE	SOURCE	IDENTIFIER
Biological samples		
<i>Anagrous</i> Haliday (Hymenoptera: Mymaridae) samples	Collected by net-sweeping from the grape fields in Ya'er County, Xinjiang Uygur Autonomous Region, China.	N/A
Software and algorithms		
Origin 8.5	Graphing and data analysis software	https://www.originlab.com/
Ansys 17.2	Ansys Inc.	https://www.ansys.com/
MATLAB2015b	Mathworks Inc.	https://www.mathworks.com/
Autodesk Computer Aided design 2014	Autodesk Inc.	https://www.autodesk.com.cn/
Solidworks2014	Dassault Systèmes Solid Works Corp.	https://www.solidworks.com/zh-hans
Other		
Piezoresistive microcantilever	SCL-Sensor. Tech. Fabrication GmbH	PRS-L450-F30-TL-PCB/CHP
Bench-top wind tunnel	OMEGA	WT4401-D
Data acquisition board	Advantech Co., Ltd.	USB-4711A 12 bits
Infrared diode laser	Changchun New Industries Optoelectronics Technology Co., Ltd.	MDL-H-808-3W
SEM	FEI Company	Quanta 450 FEG
EDS	Carl Zeiss AG	Merlin Compact
AFM	Bruker Daltonics Inc.	Dimension Icon
LDV	Polytec GmbH	MSA-500

RESOURCE AVAILABILITY

Lead contact

Further information requests should be directed to the lead contact, Professor Hao Liu (hliu@faculty.chiba-u.jp).

Materials availability

This study did not generate new unique reagents.

Data and code availability

- Original data reported in this paper will be shared by the lead contact upon request.
- This paper does not report original code.

EXPERIMENTAL MODEL AND SUBJECT DETAILS

Anagrous Haliday (Hymenoptera: Mymaridae) samples were collected by net-sweeping from the grape fields in Ya'er County, Xinjiang Uygur Autonomous Region, China. The wasps used in this experiment were within one week after birth and sex of animals was male. The tiny wasps, along with other insects and leaves were stored in 100% ethanol immediately. The animals were picked out of the mixture by using tweezers under a stereomicroscope and then stored in 70% ethanol. All the animal protocols were approved by the Biological and Medical Ethics Committee of Beihang University with authorization number of BM20210089.

METHOD DETAILS

SEM and EDS

The tiny wasps were rinsed three times with 0.1 M phosphate-buffered saline (PBS) at pH 7.0 and then fixed in 2.5% glutaraldehyde for 24 h at room temperature. After washing three times for 15 min with 0.1 M PBS,

the specimens were dehydrated in a graded ethanol series with 30%, 60% and 90% ethanol for 10 min. The dehydrated specimens were critical-point dried for 1.5 h. Finally, the samples were analyzed by using SEM (Quanta 450 FEG, FEI Company, Oregon, USA) and EDS (Merlin Compact, Carl Zeiss AG, Jena, Germany).

Bending test using AFM

The bending test for small deflections was performed by AFM (Dimension Icon, Bruker Daltonics Inc., Massachusetts, USA). The long axes of the bristle and cantilever were placed in parallel. The bristle was deflected by a cantilever that was perpendicular to the long axis of the bristle. Offline analyses were performed using an AFM data processing software package (Nano Scope Analysis, version 1.7).

LDV measurement

A wing of the insect was separated from its body by using an insect needle and was then glued to the edge of a piezoelectric actuator. To suppress the modal coupling from the wing membrane, the whole membrane was stuck on the piezoactuator and the bristles were left hanging outside. Vibrations were generated by the piezoelectric actuator, and the real-time frequency response of the bristle was obtained by LDV (Polytec, MSA-500, Irvine, CA, USA), with the laser beam (wavelength 632.8 nm, power <1 mW) focused through a $\times 50$ microscope objective on the tip of the bristle. To evaluate the bristles with various lengths, the bristles were trimmed by using an infrared diode laser (MDL-H-808-3W, Changchun New Industries Optoelectronics Technology Co., Ltd.) attached to a microscope with a $\times 50$ objective lens.

Fluid-bristle interaction analysis

The 3DFSI simulation was performed using the commercial software Ansys 17.2 (Ansys Inc.). Both the conical tubular model and cylindrical tubular model were built using the commercial software Solid-Works2014 and then imported into Ansys Workbench for FSI simulation. The computational domain was set to be $8L \times 8L \times 2.7L$ to ensure that steady calculation results were obtained.

CFD modeling of flapping-wing flight

The unsteady aerodynamics of three wing models with realistic configurations of the wing and bristles were analyzed through the CFD modeling of the flapping wing flight (hovering) of a tiny wasp using the commercial software Ansys Fluent 17.0 (Ansys Inc.). The flapping-wing kinematics were prescribed in terms of three Euler angles of the wing—the positional angle (stroke), elevation angle (deviation), and feathering angle (pitch)—as defined in a previous paper (Liu et al., 2016). These angles were based on the wing kinematics of wasps (Cheng and Sun, 2018).

QUANTIFICATION AND STATISTICAL ANALYSIS

This study does not include statistical analysis or quantification.